Global and Planetary Change 268 (2027) 105791

Contents lists available at ScienceDirect

Global and Planetary Change

journal homepage: www.elsevier.com/locate/gloplacha

Research Article

Spatial heterogeneity of marine nitrogen cycling during the Paleocene–Eocene Thermal Maximum

Jingxin Jiang [a], Xiumian Hu [a,*], Zhong Han [b], Thomas J. Algeo [c,d,e], Xi Chen [f], Eduardo Garzanti [g]

[a] State Key Laboratory of Critical Earth Material Cycling and Mineral Deposits, Key Laboratory of Surficial Geochemistry (Ministry of Education), School of Earth Sciences and Engineering, Nanjing University, Nanjing 210023, China
[b] State Key Laboratory of Palaeobiology and Stratigraphy, Nanjing Institute of Geology and Palaeontology, Chinese Academy of Sciences, Nanjing 210008, China
[c] Department of Geosciences, University of Cincinnati, Cincinnati, OH 45221, USA
[d] State Key Laboratory of Geomicrobiology and Environmental Changes, China University of Geosciences, Wuhan 430074, China
[e] State Key Laboratory of Oil and Gas Reservoir Geology and Exploitation, Chengdu University of Technology, Chengdu 610059, China
[f] State Key Laboratory of Biogeology and Environmental Geology, China University of Geosciences, Beijing 100083, China
[g] Laboratory for Provenance Studies, Department of Earth and Environmental Sciences, Università di Milano-Bicocca, Milano 20126, Italy

ARTICLE INFO

Editor: Maoyan Zhu

Keywords:
PETM
Nitrogen isotopes
Tibet
Shenkezha
Pyrenees
Campo

ABSTRACT

Modern global warming is reshaping marine nitrogen cycling and ocean biogeochemistry. Investigating nitrogen cycling during past hyperthermal events, such as the Paleocene-Eocene Thermal Maximum (PETM), provides insights into future climate dynamics. Nitrogen-isotope records from two shallow-marine carbonate successions: the Campo section (Spain) and the Shenkezha section (Tibet, China) show relatively stable and elevated organic nitrogen-isotopic compositions ($\delta^{15}N_{org}$) during the PETM, in contrast to the predominantly negative $\delta^{15}N_{org}$ or foraminifera-bound $\delta^{15}N$ excursions previously reported from open-ocean, restricted-basin, and marginal-marine sites. Elevated $\delta^{15}N_{org}$ values at Campo are ascribed to enhanced nutrient supply and productivity, mild water-column deoxygenation, and a regionally ^{15}N-enriched nitrate supply. At Shenkezha, instead, a slight $\delta^{15}N_{org}$ decrease during the PETM core and a positive excursion in the recovery stage reflect pore-water anoxia and redox fluctuations at the sediment-water interface. These records suggest that nitrogen cycling in shallow-marine carbonate platforms remained largely nitrate-based and was mainly controlled by local nitrate utilization and denitrification in the water column or sediments. Further comparisons indicate that PETM marine nitrogen cycling was spatially heterogeneous, reflecting regional differences in productivity, oxygen levels, hydrography, nutrient sources, and depositional setting. Against this heterogeneous background, well-ventilated shallow-water carbonate platforms may have acted as regional biogeochemical buffers, sustaining nitrate-based ecosystems during widespread nitrogen-cycle disruption.

1. Introduction

Modern global warming is altering marine nitrogen cycling by reducing ocean oxygenation, strengthening stratification, and reorganizing nutrient supply (Hutchins and Capone, 2022). Tracking nitrogen cycling thus provides crucial insights into marine biogeochemistry. The responses related to nitrogen cycling, however, are spatially variable, hampering robust predictions of their behavior under continuing warming. The Paleocene-Eocene Thermal Maximum (PETM; ~56 Ma) was the largest and fastest known pre-anthropogenic global-warming event in the Cenozoic (Kennett and Stott, 1991; Zachos et al., 2001). The PETM was associated with a massive release of isotopically light carbon into the ocean–atmosphere system, producing a rapid negative carbon-isotope excursion (PETM Onset), followed by an interval of persistently low $\delta^{13}C$ values (PETM Body) and by a subsequent positive shift toward pre-event values (PETM Recovery; McInerney and Wing, 2011). The environmental changes included rapid warming, ocean acidification, and disruption of the hydrological cycle (Zachos et al., 2005; Aze et al., 2014; Carmichael et al., 2017; Xu et al., 2025; Jiang et al., 2026). Because the amplitude of the temperature increase is comparable with that of the future RCP8.5 carbon-emission scenario (Tierney et al., 2022), the PETM is widely regarded as one of the best

* Corresponding author.
E-mail address: huxm@nju.edu.cn (X. Hu).

https://doi.org/10.1016/j.gloplacha.2026.105791
Received 9 August 2026; Received in revised form 25 September 2026; Accepted 30 October 2026
Available online 1 November 2026
0921-8181/© 2026 Elsevier B.V. All rights are reserved, including those for text and data mining, AI training, and similar technologies.

analogues for investigating the future state of marine nitrogen cycling.

Nitrogen isotopes ($\delta^{15}N$) are valuable tracers due to their sensitivity to changes in nitrogen-cycling processes, including nitrogen fixation, nitrification, denitrification, and anammox in the water column or sediments (Stüeken et al., 2016, 2024; Chang and Algeo, 2025). Generally, water-column denitrification in oxygen-deficient zones (ODZs) preferentially removes ^{14}N from nitrate, enriching the residual nitrate pool in ^{15}N and thereby increasing the $\delta^{15}N$ of exported organic matter (Algeo et al., 2008). In contrast, sedimentary denitrification generally produces a weaker isotopic effect because nitrate consumption in pore waters is nearly complete. Nitrogen fixation supplies isotopically light nitrogen, with $\delta^{15}N$ values close to atmospheric N_2, whereas ammonium accumulation and photic-zone ammonium assimilation under strongly reducing conditions can produce even lower $\delta^{15}N$ values in sedimentary deposits (Stüeken et al., 2016, 2024; Chang and Algeo, 2025). Beyond these process-specific isotopic effects, the $\delta^{15}N$ of marine fixed nitrogen also varies systematically among oceanic basins. In the modern ocean, relatively low values in the tropical and subtropical North Atlantic reflect the remineralization of isotopically light organic matter derived from N_2 fixation, whereas elevated values in much of the tropical Indo-Pacific mainly result from strong denitrification (Rafter et al., 2012; Marconi et al., 2015; Rafter et al., 2019). These regional signatures are transported and modified by mixing and remineralization along thermocline, intermediate-water, and deep-water circulation pathways. Consequently, site-specific $\delta^{15}N$ dose not only reflect local biogeochemical variations but also the isotopic composition of the source watermass and cumulative alteration during watermass transport.

Recent records of nitrogen isotopes from PETM sections have revealed significant spatial variability in marine response. In the tropical North Pacific, a decline in foraminifera-bound $\delta^{15}N$ (FB-$\delta^{15}N$ or $\delta^{15}N_{foram}$) during the PETM has been interpreted to reflect contraction of ODZs, along with reduced water-column denitrification, decreased productivity, and increased oxygenation in the subsurface ocean (Moretti et al., 2024). In contrast, the South Atlantic shows a decline in $\delta^{15}N_{foram}$ that correlates with enhanced export productivity. This pattern has been interpreted as an expansion of ODZs from suboxic to anoxic conditions in the thermocline, along with the development of ammonium-type ODZs (Yao et al., 2024). The nitrogen records in continental-marginal and restricted-marine basins further demonstrate that PETM nitrogen-cycle perturbations were highly sensitive to local hydrography and nutrient supply. Along the southern Tethyan margin of northeastern Africa, the Wadi Nukhul and EI Dababiya sections in Egypt exhibit significant negative shifts in $\delta^{15}N_{org}$ during the PETM, indicative of blooms of N_2-fixing cyanobacteria (Khozyem et al., 2013, 2015). At Kheu River in the Eastern Peri-Tethyan domain, $\delta^{15}N_{org}$ values decreased markedly during the PETM within an organic-rich sapropel, with Fe-speciation and sedimentological evidence indicating anoxic to euxinic conditions. Such an extreme depletion in $\delta^{15}N_{org}$ was attributed to the assimilation of recycled ammonium in the photic zone, which occurred alongside increased stratification of the water column driven by enhanced runoff and nutrient input (Junium et al., 2018a).

Despite these advances, the nitrogen-cycle response of shallow-marine carbonate platforms during the PETM remains poorly constrained. Carbonate platforms are more sensitive than open-marine settings to runoff and nutrient delivery, local circulation, carbonate production, and redox processes at the sediment-water interface. Determining whether such settings recorded the global ocean $\delta^{15}N$ decrease, restricted-basin N_2 fixation, ammonium assimilation, or a distinct shallow-platform signal is therefore essential for resolving the spatial structure of PETM nitrogen cycling (Khozyem et al., 2013, 2015; Junium et al., 2018a; Moretti et al., 2024; Yao et al., 2024). We here present paired nitrogen-isotope and geochemical records from two shallow-marine carbonate profiles: the Campo section in the Pyrenees (Li et al., 2021) and the Shenkezha section in southern Tibet (Li et al., 2020), to explore the dynamic changes of nitrogen cycling and its implications for the environmental evolution of carbonate platforms during the PETM.

2. Geological setting

The Shenkezha section (N 28°41′33.0″, E 86°43′02.6″), located in the Tingri area of southern Tibet, is part of the Tethys Himalaya Zone, which contains the remnants of the passive continental margin of northern India facing the Neo-Tethys Ocean (Fig. 1; Yi et al., 2011; Sciunnach and Garzanti, 2012; Garzanti, 2026). During the early Paleogene, shallow-water carbonate platforms developed in the south and deep-water facies in the north of the Tethys Himalaya (Wang et al., 2011; Hu et al., 2012; Li et al., 2015). The uppermost Paleocene to lowermost Eocene succession exposed at Shenkezha (Zongpu Formation) consists of a ~ 18-m-thick nodular limestone and marly limestone overlain by ~6 m of thick-bedded to massive limestone, as documented in detail by Li et al. (2020). A prominent negative carbon isotope excursion (CIE), together with benthic foraminiferal biostratigraphy, indicates that these strata record the PETM event. Microfacies analysis suggests that the PETM interval was associated with a transgression during its initial phase and main body, followed by regression during the recovery phase. This evolution exerted an important control on benthic faunal assemblages and terrigenous fluxes in the Shenkezha shallow-marine platform (Li et al., 2020, 2022; Jin et al., 2023).

The Campo section (N 42°23′17.4″, E 00°23′52.9″) is located in the Pyrenees of northern Spain (Fig. 1), a ~ 400-km-long fold-and-thrust belt produced by convergence between Eurasia and Iberia (Roest and Srivastava, 1991). During the early Paleogene, the Pyrenean domain included a deep-water gulf opening westward into the Bay of Biscay and bordered by shallow-marine carbonate platforms (Plaziat, 1981). The Campo section was deposited in the Tremp-Graus Basin at the southeastern margin of this gulf (Payros et al., 2000; Scheibner et al., 2007). The Paleocene-Eocene interval here comprises three major lithostratigraphic units: i) pre-PETM transgressive inner-ramp deposits of the upper Navarri Formation; ii) *syn*-PETM mixed carbonate-siliciclastic deposits of the Claret Formation; and iii) post-PETM renewed carbonate-ramp deposits of the lower Serraduy Formation. These three units are separated by unconformable surfaces that mark major changes in depositional regime (Pujalte et al., 2014; Li et al., 2021). The temporary demise of carbonate-ramp sedimentation during the PETM has been attributed to enhanced siliciclastic input induced by a major intensification of the hydrological cycle (Li et al., 2021).

3. Materials and methods

Organic nitrogen isotope ($\delta^{15}N_{org}$) analyses were performed for both the Campo and Shenkezha sections on samples studied by Li et al. (2020, 2021). For the Campo section, organic carbon isotopes, major and trace elements, total carbon (TC), and total nitrogen (TN) were also analyzed (Tables S1-S3). For the Shenkezha section, previously published C/N ratios, TC, and TN data from Li et al. (2020), together with comparable data from Jiang et al. (in review), were compiled for comparison.

Organic-matter nitrogen- and carbon-isotope analyses were conducted at International Center for Isotope Effects Research, Nanjing University, using a Thermo Scientific Flash 2000 Elemental Analyzer coupled with a Thermo Scientific DELTA V Plus isotope ratio mass spectrometer. The powdered samples were decalcified using 2 M HCl. The solutions were washed to remove chloride residues and dried overnight at 60 °C. About 20–30 mg of the acid residue was weighed and placed into a tin capsule loaded into an auto-sampler for nitrogen-isotope analyses. The reaction tube was maintained at a temperature of 960 °C, with a helium carrier gas flow rate of 90 mL/min. The $\delta^{15}N$ values were reported by single-point calibration using the laboratory internal standard Acetanilide ICIER-ACE-1 ($\delta^{15}N = -2.78‰$ *vs* air), with sample analytical precision better than ±0.2‰. The $\delta^{13}C$ values are expressed as per mill deviations from the Vienna Pee Dee Belemnite

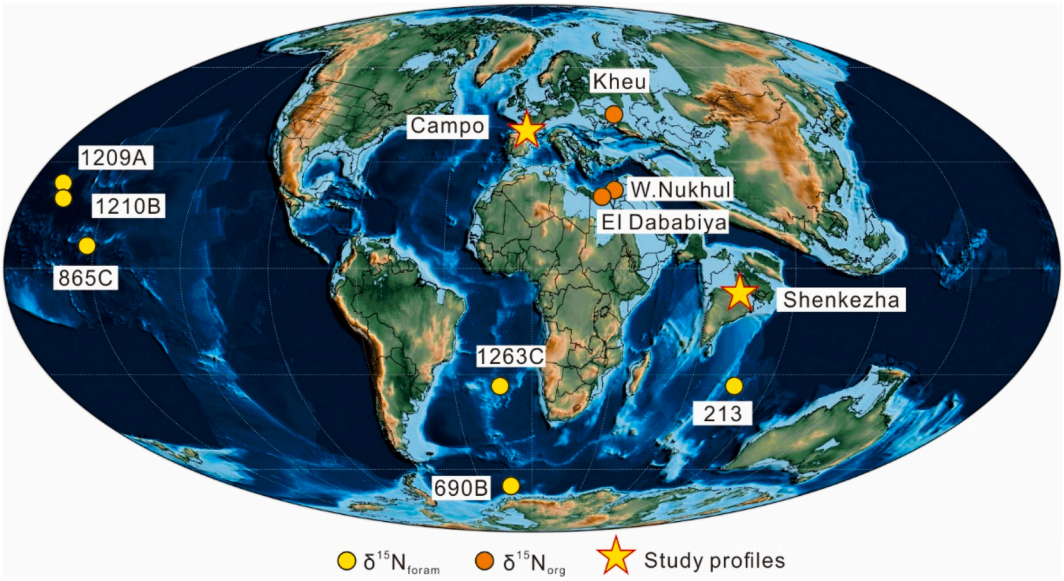


Fig. 1. Global paleogeography at ~56 Ma (Scotese, 2021), illustrating the studied PETM sections and additional sites yielding nitrogen isotope data.

(VPDB) standard. Duplicate measurements of standards yielded an analytical precision of 0.1‰ (1σ). Analytical precision for total carbon (TC) and total nitrogen (TN) was better than 0.01% and 0.02%, respectively. Total organic carbon (TOC) was calculated by subtracting total inorganic carbon (TIC) from TC; C: N molar ratios were calculated using TOC and TN corrected for the molar weight of C and N, respectively.

Analyses of major and trace elements were made at the Nanjing Institute of Geology and Palaeontology, Chinese Academy of Sciences. About 50 mg of powdered carbonate-rock sample were weighed and dissolved overnight in 3 mL of 0.5-M acetic acid prepared with distilled water. After dissolution, the samples were centrifuged, and the supernatant was transferred to a clean beaker. The insoluble residues were weighed and rinsed three times with ultrapure water, and the rinsing solutions were combined with the corresponding supernatant. The resulting leachates were then converted to a nitric acid medium before analysis. Major-element concentrations were measured using an Agilent 710 inductively coupled plasma optical emission spectrometer (*ICP-OES*), with analytical precision better than 5%. Trace-element concentrations were determined using an Agilent 7700 A inductively coupled plasma mass spectrometer (*ICP-MS*), with analytical precision better than 2%. The cerium anomaly (Ce/Ce*) was calculated from rare earth element (REE) concentrations normalized to PAAS (Post-Archean Australian Shale standard of Taylor and McLennan, 1985). Ce/Ce* reflects the relative depletion or enrichment of PAAS-normalized Ce ($[Ce]_N$) relative to neighboring, non-redox-sensitive REEs (Lawrence et al., 2006).

4. Results

4.1. Campo section

In the Campo section, the $\delta^{15}N_{org}$ values are relatively low (+1 to +3‰) below the PETM, but increase significantly to +4–6‰ in the PETM interval, and decrease slightly to ~+3.5‰ above. The TN content is low (< 0.04%), without significant enrichment in TOC (from 0.02% to 1.70%). The molar C/N ratio decreases from ~37 below the PETM to ~6 in the PETM interval, rising again up to 46 above. The Y/Ho ratio declines from ~52 below the PETM to ~35 during the event, followed by a partial recovery to ~41. The Ba/Al ratio, largely stable below 0.04, also shows a sharp increase to ~0.14 at PETM onset. The P/Ca ratio mostly ranges from 0 to 200 (average ~60), reaching the highest values in the PETM interval (Fig. 2; average ~186).

4.2. Shenkezha section

The $\delta^{15}N_{org}$ values remain relatively constant in the lower part of the Shenkezha section, decreasing only slightly from ~+5.5‰ before the PETM to ~+4.8‰ in the core of the PETM interval. A noticeable increase to +8–10‰ is observed during the later phase of the PETM body stage, followed by a return to background levels of +3–5‰ above the PETM. The TN content ranges from 0.05% to 0.22%, showing a slight decline during the PETM. The TOC content fluctuates between 0.05% and 0.38% through the PETM interval. The C/N ratio declined from ~14 below the PETM to ~5 in the PETM interval (Li et al., 2020). The Y/Ho ratio varies between 32 and 42 but mostly remains above 36. Both Zn/Ca and Ba/Al ratios are relatively constant but show an increase during the recovery stage (Fig. 2).

5. Discussion

5.1. Preservation of primary geochemical signatures

Before using the $\delta^{15}N_{org}$ records to infer changes in nitrogen cycling, we must first evaluate whether the isotopic signals could have been modified by organic-matter degradation, source mixing, inorganic nitrogen contribution, or early diagenesis (Fig. 3; Ader et al., 2014; Stüeken et al., 2016, 2024).

In the Campo section, TOC and TN show a moderately positive correlation ($R^2 = 0.302$, $p < 0.001$), suggesting that the nitrogen content is mainly associated with organic matter, although other forms of nitrogen may have contributed (Fujisaki et al., 2019). The weak correlation between C/N and TOC ($R^2 = 0.247$, $p < 0.001$), together with relatively high C/N ratio in some samples, suggest variable organic-matter preservation and/or source mixing. Nevertheless, $\delta^{15}N_{org}$ shows no correlation with TOC ($R^2 < 0.001$, $p = 0.984$), TN ($R^2 = 0.068$, $p = 0.071$) and $\delta^{13}C_{org}$ ($R^2 = 0.061$, $p < 0.064$; Ader et al., 2014; Wang et al., 2018) and a weak negative correlation with C/N ($R^2 = 0.268$, $p < 0.001$), which is inconsistent with diagenetic enrichment of residual organic nitrogen in ^{15}N (Robinson et al., 2012). Although a few Campo samples may have been partly affected by preservation or source-mixing effects, the positive excursion in $\delta^{15}N_{org}$ during the PETM cannot be explained by diagenetic processes.

In the Shenkezha section, TOC and TN are uncorrelated ($R^2 = 0.026$,

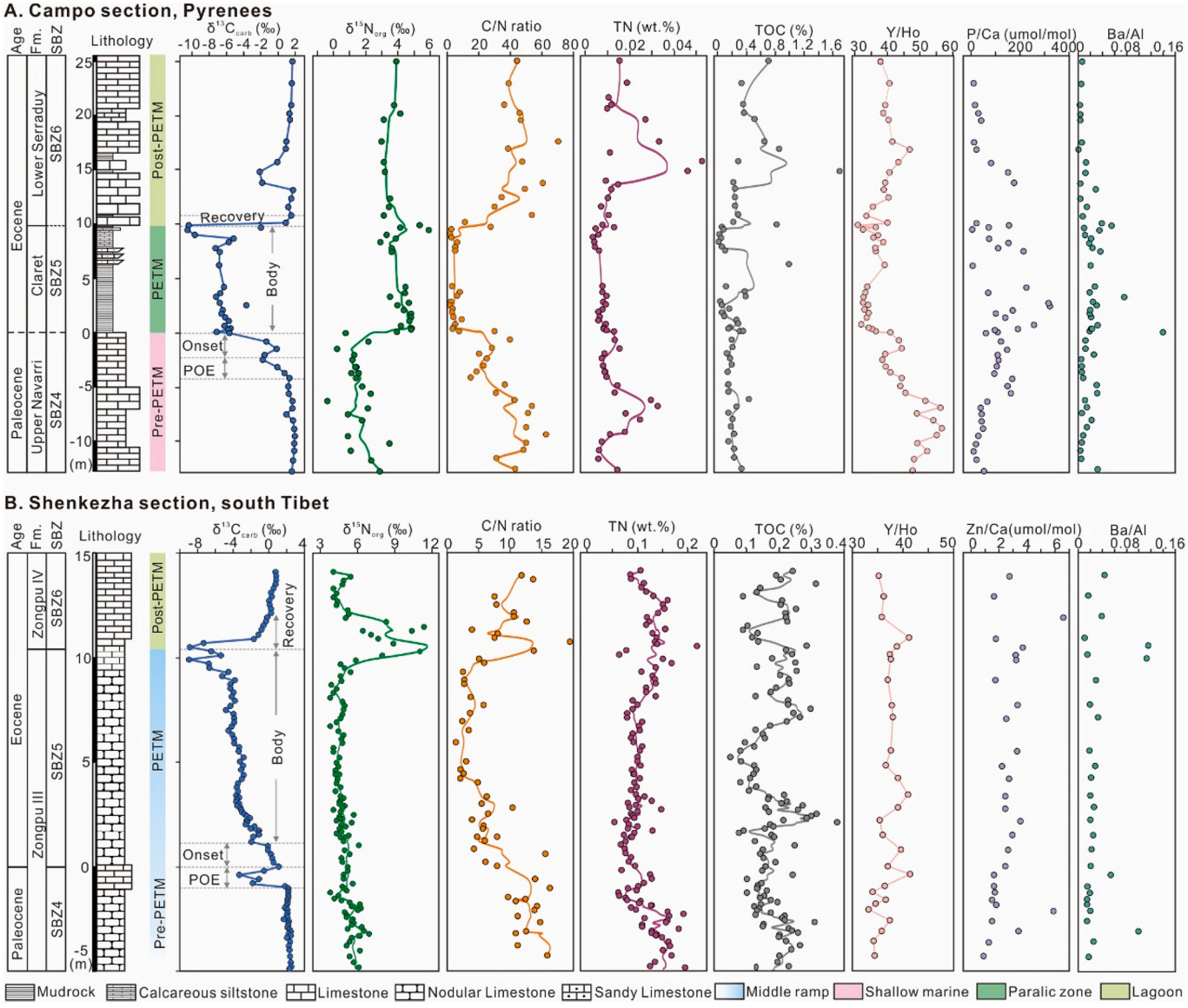


Fig. 2. Stratigraphic logs of Campo and Shenkezha sections showing trends of various geochemical proxies. The $\delta^{13}C_{carb}$ curves for Campo are from Li et al. (2021), $\delta^{13}C_{carb}$, C/N, TN %, and TOC % data for Shenkezha from Li et al. (2020) and Zn/Ca and Ba/Al data for Shenkezha from Jiang et al. (in review). POE: pre-onset excursion.

$p = 0.065$), suggesting that variations in TN were not controlled solely by organic-matter abundance (Fujisaki et al., 2019). The $\delta^{15}N_{org}$ profile shows no significant correlation with TOC ($R^2 = 0.023$, $p = 0.087$) or $\delta^{13}C_{org}$ ($R^2 = 0.011$, $p = 0.238$), and only a weak correlation with TN despite its statistical significance ($R^2 = 0.102$, $p < 0.001$), suggesting that the nitrogen-isotope record was not systematically controlled by organic-matter abundance, nitrogen concentration, or organic-carbon source (Ader et al., 2014; Wang et al., 2018). The very weak relationship between $\delta^{15}N_{org}$ and C/N ($R^2 = 0.180$, $p = 0.001$) might reflect limited organic-matter degradation or nitrogen loss in some samples, an effect much too weak to explain the main $\delta^{15}N_{org}$ pattern (Robinson et al., 2012; Yang et al., 2021). Both records from Campo and Shenkezha sections, therefore, retain meaningful depositional signals that can be used to evaluate shallow-marine nitrogen cycling during the PETM.

Elemental ratios, such as P/Ca, Zn/Ca, and Ba/Al, used to evaluate nutrient availability and productivity can also be influenced by variations in carbonate abundance, detrital input, and early diagenesis (Dymond et al., 1992; Gonneea and Paytan, 2006; Tribovillard et al., 2006). We therefore investigated these potential controls based on correlation analysis (Fig. S1).

Phosphorus incorporation into carbonate is sensitive not only to ambient phosphate availability but also to carbonate mineralogy, and post-depositional alteration (Dodd et al., 2021). At Campo, P concentration shows no significant relationship with Ca ($R^2 = 0.023$, $p = 0.290$), suggesting that variations in P abundance were not simply controlled by carbonate abundance. Sedimentary Ba likewise occurs in multiple phases, including marine barite, carbonate, organic matter, and detrital aluminosilicates (Gonneea and Paytan, 2006). Ba is negatively correlated with Ca at Campo ($R^2 = 0.466$, $p < 0.001$), arguing against a simple control of Ba accumulation by carbonate abundance, whereas a slightly positive relationship with Al ($R^2 = 0.231$, $p < 0.001$) indicates that a detrital contribution was limited but cannot be excluded. At Shenkezha, Ba shows no significant relationship with either Ca ($R^2 = 0.015$, $p = 0.501$) or Al ($R^2 = 0.003$, $p = 0.790$), suggesting that neither carbonate abundance nor detrital input exerted a simple first-order control on the Ba record. Zn is likewise unrelated to Ca at Shenkezha ($R^2 = 0.019$, $p = 0.457$). These relationships indicate that carbonate dilution cannot account for the observed elemental variations.

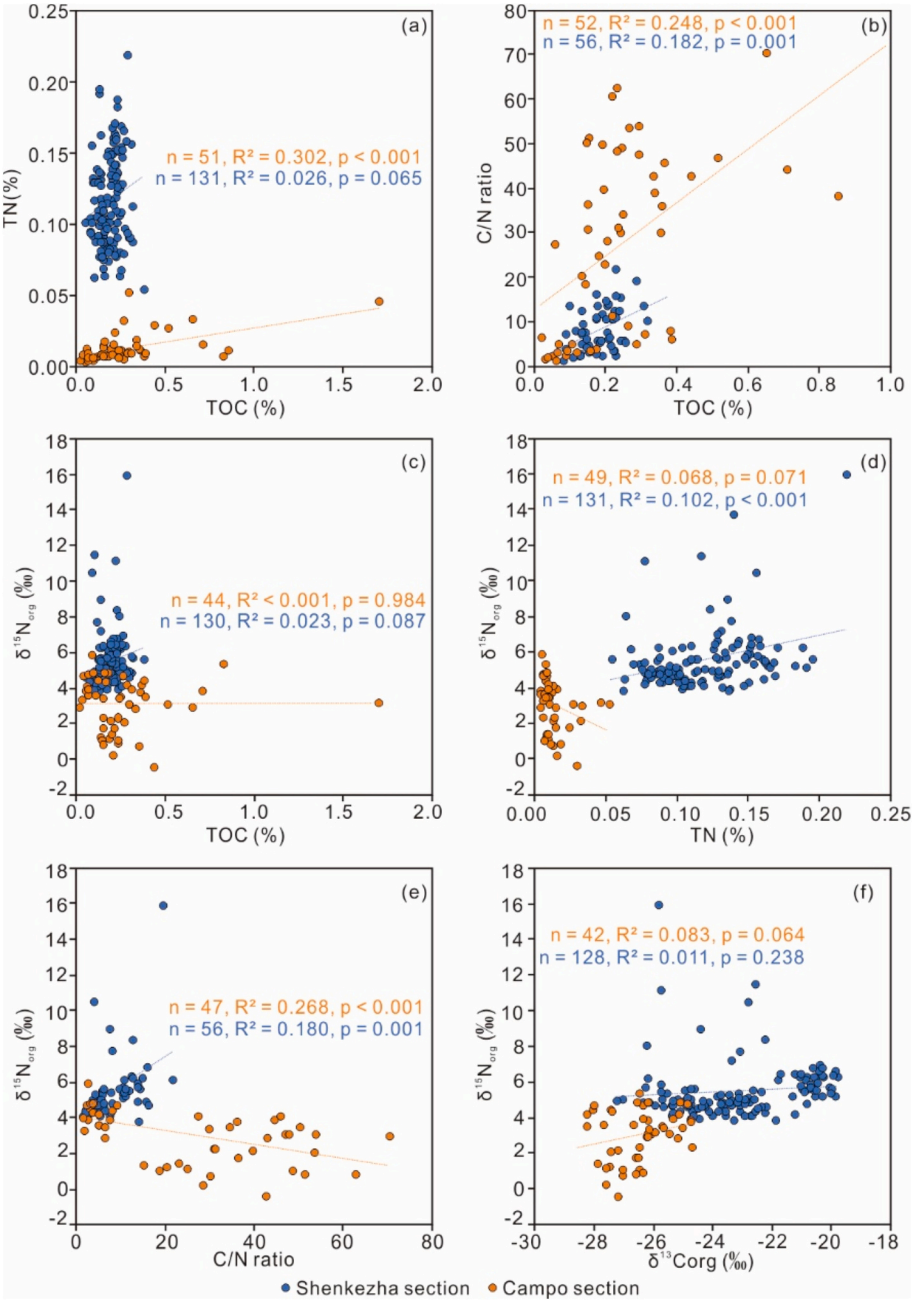


Fig. 3. Crossplots of isotopic values and elemental concentrations for Campo and Shenkezha sections with number of effective data points (n), R^2, and *p*-values: a) TN ‰ *vs.* TOC %; b) C/N *vs.* TOC %; c) $\delta^{15}N_{org}$ ‰ *vs.* TOC %; d) $\delta^{15}N_{org}$ ‰ *vs.* TN %; e) $\delta^{15}N_{org}$ ‰ *vs.* C/N; f) $\delta^{15}N_{org}$ ‰ *vs.* $\delta^{13}C_{org}$ ‰. TOC, TN and C/N data from Shenkezha section are from Li et al. (2020).

We conclude that stratigraphic trends in P/Ca, Ba/Al, and Zn/Ca reliably reflect changes in nutrient availability and productivity.

5.2. Nitrogen cycling on carbonate platforms during the PETM

Sedimentary organic nitrogen typically reflects the isotopic signature of fixed ions (*e.g.*, NO_3^-, NO_2^-, and NH_4^+) from the watermass of origin (Stüeken et al., 2016, 2024). The residence time of fixed nitrogen in the modern ocean is less than 3 kyr (Gruber and Sarmiento, 1997; Stüeken et al., 2024), similar to the timescale of oceanic mixing, which results in spatial variations in isotopic composition. In addition, the localized effects of fractionation during nitrogen fixation, nitrification, denitrification, and assimilatory uptake further contribute to these isotopic variations (Jenkyns et al., 2001; Stüeken et al., 2016, 2024). Biological nitrogen fixation (diazotrophy; reduction of N_2 to NH_4^+) imparts a small fractionation, with a range from −2‰ to +1‰ (−1‰ on average), and lowers the $\delta^{15}N$ of seawater nitrate (Zerkle et al., 2008; Zhang et al., 2014). In the presence of O_2, even at nM O_2 levels in marine ODZs, the fixed NH_4^+ is quickly re-oxidized to NO_2^- and NO_3^- through nitrification, resulting in the NO_3^- pool being isotopically lighter than the original biomass (Casciotti et al., 2003; Casciotti, 2009; Füssel et al., 2012). In contrast, under suboxic conditions, denitrification involves bacteria that preferentially utilize ^{15}N-depleted nitrate as an oxidant, resulting in a fractionation range of −22‰ to −30‰. This process can lead to a watermass with residual nitrate significantly enriched in ^{15}N (Altabet et al., 1995). Sedimentary denitrification, however, does not lead to strong fractionation because of generally complete consumption of NO_3^- (Brandes and Devol, 2002). Fractionation associated with NO_3^-

assimilation is generally minor, because assimilation typically proceeds to completion (Thunell et al., 2004), except in low-productivity settings where the fractionation associated with assimilatory uptake can reach −5‰ (Sigman et al., 1999). Anaerobic ammonium oxidation coupled with nitrite reduction (anammox) contributes to the overall rates of denitrification in seawater, but its impact on the isotopic composition of bioavailable nitrogen is considered minimal (Kalvelage et al., 2013). NH_3 volatilization requires sustained high alkalinity and strongly restricted or evaporative conditions, preferentially removing ^{14}N and thus leading to an increase in $\delta^{15}N$ (Stüeken et al., 2015).

In the Campo section, the $\delta^{15}N_{org}$ profile shows a positive excursion, with average values increasing from ~+1.6‰ below the PETM to ~+4.3‰ in the PETM interval, indicating that the regional bioavailable fixed-N pool became isotopically heavier during the event (Fig. 2). The relatively low pre-PETM $\delta^{15}N_{org}$ values may indicate some contribution from N_2 fixation, whereas the significantly higher $\delta^{15}N$ values during the PETM suggest that N_2 fixation was not a major source of bioavailable nitrogen (Zerkle et al., 2008). NH_3 volatilization could be ruled out because the Campo section documents a shallow-water environment with good circulation where such a process can hardly occur (Li et al., 2021). Anammox is not considered here because the redox conditions did not reach an anoxic level (Mulder et al., 1995; Li et al., 2021). The decrease in Y/Ho during the PETM is consistent with increased terrestrial or detrital influence (Tostevin et al., 2016), in agreement with the facies transition associated with an intensified hydrological cycle (Li et al., 2021). In contrast, the concomitant decrease in C/N argues against a dominant increase in land-plant inputs and may instead reflect greater nitrogen enrichment of predominantly marine organic matter (Meyers, 1997). Notably, although the relatively low TN contents during the PETM may have affected the C/N ratio, they do not readily explain its overall decrease. Marine particulate organic matter can exhibit variable C/N ratios in response to fixed-N availability, with stronger N limitation generally producing N-poor organic matter with higher C/N ratios, and *vice versa* (Geider and La Roche, 2002; Martiny et al., 2013). The lower C/N values during the PETM may therefore suggest a greater availability of bioavailable fixed nitrogen or reduced nitrogen limitation in surface waters, plausibly supported by enhanced runoff-derived nutrients (Soliman et al., 2011; Martiny et al., 2013). The simultaneous increase in P/Ca and Ba/Al ratios are broadly consistent with enhanced nutrient availability and productivity (Figs. 2, S1; Schoepfer et al., 2015; Tostevin et al., 2016). The higher nitrate availability may have reduced the relative contribution of newly fixed, low-$\delta^{15}N$ nitrogen to the bioavailable N pool, consistent with the observed positive $\delta^{15}N_{org}$ at Campo during the PETM. Additionally, regional deoxygenation during the PETM driven by warming-induced reductions in oxygen solubility and enhanced export productivity may have expanded nitrate-bearing suboxic waters, promoting incomplete water-column denitrification and preferential removal of ^{14}N (Clarkson et al., 2021; Yao et al., 2024). The resulting ^{15}N-enriched residual nitrate could then have been transported to Campo by regional circulation and assimilated by marine primary producers. Collectively, the evidence suggests that enhanced nutrient supply reduced nitrogen limitation at Campo, whereas the positive $\delta^{15}N_{org}$ excursion primarily records the influence and assimilation of an isotopically heavy regional nitrate pool (Brandes and Devol, 2002). The persistence of elevated $\delta^{15}N_{org}$ above the PETM interval suggests that this isotopically heavy regional fixed-N pool continued to influence the Campo platform after the event.

In the Shenkezha section, $\delta^{15}N_{org}$ values exhibit a two-stage evolution through the PETM, characterized by a prolonged interval of stable to slightly decreasing values followed by a positive excursion during PETM recovery (Fig. 2). The persistently elevated $\delta^{15}N_{org}$ values (average ~+5.5‰) in this carbonate-ramp setting with good water circulation indicate that N_2-fixation and NH_3 volatilization unlikely took place (Li et al., 2020). The decrease in C/N and the increase in Y/Ho are consistent with reduced detrital influence and a stronger marine signature during the PETM transgression (Tostevin et al., 2016; Li et al., 2020). Larger benthic foraminifera remained very abundant throughout the PETM interval, which suggests that bottom waters were generally well oxygenated, arguing against persistent water-column anoxia (Li et al., 2020; Zhang et al., 2023). In contrast, pore-water deoxygenation in the region during the PETM has been identified by the analysis of $\delta^{238}U$ and U/Th (Zhang et al., 2023). The absence of coherent first-order changes in Zn/Ca and Ba/Al likewise provides no clear evidence for a major sustained change in productivity, although their fluctuations in the PETM recovery may indicate short-lived variability (Figs. 2, S1; Morel and Price, 2003; Paytan et al., 2007). The stable to slightly decreasing $\delta^{15}N_{org}$ values during the pre-PETM and PETM-core intervals, therefore, most conservatively reflect a stable or reduced isotopic imprint of water-column denitrification and a potential greater role of sedimentary denitrification in pore water. Because nitrate diffusing into reducing sediments is efficiently consumed, sedimentary denitrification generally produces only a limited isotopic effect on the overlying dissolved nitrogen pool (Brandes and Devol, 2002). During PETM recovery, the increase in $\delta^{15}N_{org}$ is accompanied by fluctuating Zn/Ca and Ba/Al ratios. In addition, relative sea-level fall at this stage may have enhanced sediment-water exchange, promoted the upward migration of reducing pore-water signals, and favored the transient development of suboxic conditions near the sediment-water interface (Li et al., 2020; Zhang et al., 2023). During regression, erosion and increasing supply of terrigenous detritus may have led to increased nutrient supply (Hunt and Tucker, 1992; Carmichael et al., 2017). The expanded nutrient pool and enhanced suboxic conditions may have promoted denitrification in the water column or near the sediment-water interface, enriching the residual dissolved nitrogen pool in ^{15}N and thereby contributing to the positive $\delta^{15}N_{org}$ excursion (Altabet et al., 1995; Brandes and Devol, 2002).

Overall, the $\delta^{15}N_{org}$ trends in the Campo and Shenkezha PETM sections indicate that nitrogen cycling was spatially heterogeneous in carbonate platforms. At Campo, increased runoff likely enhanced nutrient delivery and nitrate availability, which along with potential mild water-column deoxygenation promoted sustained denitrification and enriched the bioavailable nitrogen pool in ^{15}N. In contrast, the environmental conditions at Shenkezha remained generally well oxygenated during the PETM core interval, and denitrification was largely restricted to reducing pore waters, with limited isotopic overprint. During the recovery phase, the regression, along with increased terrestrial input and temporary suboxic conditions near the sediment-water interface likely enhanced denitrification, leading to a positive $\delta^{15}N_{org}$ excursion. These records suggest that PETM carbonate platforms recorded site-specific nitrogen-cycle responses governed by the coupling of runoff, productivity, sea-level change, and redox dynamics.

5.3. Global evaluation of nitrogen cycling during the PETM

5.3.1. Inferences based on $\delta^{15}N$ heterogeneity of the modern ocean

In the modern ocean, the nitrogen isotopic composition exhibits considerable variability, both spatially and vertically (Rafter et al., 2019; Du et al., 2026). Generally, nitrate $\delta^{15}N$ in the well-ventilated deep ocean converges toward a global mean of ~+5‰, while it varies in the upper ocean and thermocline, where biological nitrogen transformations exert their strongest influence (Sigman et al., 2009; Tesdal et al., 2013; Rafter et al., 2019). The global compilation indicates that the tropical and subtropical North Atlantic has relatively low $\delta^{15}N_{nitrate}$ values. In contrast, the tropical Indo-Pacific and particularly the eastern tropical Pacific and the Arabian Sea exhibit elevated values (Rafter et al., 2019). This pattern of marine $\delta^{15}N_{nitrate}$ distribution serves as a spatially integrated signal shaped by the production, remineralization, and advective transport of isotopically distinct nitrogen pools (Rafter et al., 2019). The low $\delta^{15}N_{nitrate}$ values observed in the subtropical North Atlantic are commonly attributed to the remineralization of organic nitrogen ultimately derived from N_2 fixation. The export and subsequent remineralization of this isotopically light organic matter lower the

$\delta^{15}N_{nitrate}$ of subsurface nitrate. In the shallow thermocline of the western and central North Atlantic, $\delta^{15}N_{nitrate}$ declines to approximately +2.5‰ (~2.3‰ lower than deep Atlantic values), providing direct evidence for the accumulation of ^{15}N-depleted regenerated nitrogen in the subtropical thermocline. The eastern tropical Pacific constitutes an important high-$\delta^{15}N_{nitrate}$ endmember in the modern ocean. The average $\delta^{15}N_{nitrate}$ value in both thermocline and intermediate waters is ~+7.1‰, which is more than 2‰ higher than the typical values found in the deep ocean (Rafter et al., 2012). In its ODZs, water-column denitrification preferentially removes nitrate enriched in ^{14}N, which leaves behind a residual nitrate pool enriched in ^{15}N. This isotopically heavy nitrate is then transported to regions where nitrogen loss is minimal, contributing to the elevated $\delta^{15}N_{nitrate}$ values observed through much of the tropical Pacific thermocline. These basin-scale $\delta^{15}N_{nitrate}$ gradients are not generated solely by local biogeochemical processes. Ocean circulation redistributes the isotopic signatures produced by N_2 fixation, denitrification, nitrate assimilation, and remineralization beyond the regions in which they originate. During transport, these source-water signatures are further modified by watermass mixing and by the remineralization of locally and regionally produced organic matter (Rafter et al., 2012; Marconi et al., 2015; Rafter et al., 2019).

Modern marginal seas also exhibit pronounced spatial heterogeneity in sedimentary $\delta^{15}N$ (Du et al., 2026). In river-influenced settings, such as Bohai Bay and the East China Sea, inputs of ^{15}N-depleted terrestrial organic matter and clay-bound inorganic nitrogen can substantially modify the marine isotopic signal (Sun et al., 2025). In contrast, in marginal-sea regions with weaker terrigenous influence, such as the western South China Sea, sedimentary $\delta^{15}N$ more closely reflects regional marine nitrogen cycling, including nutrient utilization, N_2 fixation, remineralization, and water-mass transport (Li et al., 2019). Shallow-water carbonate environments provide another relevant example. Across globally distributed reef sites, coral skeletal $\delta^{15}N_{coral}$ varies by ~10‰ and is strongly related to the $\delta^{15}N_{nitrate}$ of subsurface nitrate supplied to the reefs, indicating that these environments can record both regional nutrient-source signatures and local biogeochemical processing (Wang et al., 2016). Restricted and strongly stratified basins exhibit distinct nitrogen-isotope signatures. For instance, in the Cariaco Basin off northern Venezuela, near-complete nitrate consumption at the oxic–anoxic interface suppresses the isotopic expression of water-column denitrification, such that sedimentary $\delta^{15}N$ largely reflects the relatively ^{15}N-depleted nature of thermocline nitrate supplied to the basin (Thunell et al., 2004). Similarly, in the Black Sea, ammonium-rich anoxic waters support coupled nitrification, anammox, and denitrification across the suboxic interface, while near-complete consumption of fixed nitrogen produces a much smaller net isotopic effect than that typical of open-ocean nitrate-type ODZs (Murray et al., 2005).

The sedimentary $\delta^{15}N$ composition recorded at any given marine site thus integrates the effects of local biogeochemical and redox processes, with regional nutrient sources, water-mass transport, terrestrial inputs, and basinal restriction. This modern-ocean framework suggests that differences in PETM $\delta^{15}N$ records may reflect not only local redox conditions, but also changes in basin-scale nutrient transport and oceanic circulation.

5.3.2. $\delta^{15}N$ heterogeneity in the PETM ocean

In this study, we compiled published marine nitrogen-isotope records of the PETM, including $\delta^{15}N_{foram}$ and organic $\delta^{15}N_{org}$, to investigate nitrate cycling modes at a basinal scale. Among them, $\delta^{15}N_{foram}$ more directly reflects the fixed-N pool in the habitat of the foraminifera, whereas $\delta^{15}N_{org}$ integrates organic N derived from multiple sources and processes and potentially influenced by terrestrial input (Ren et al., 2012; Robinson et al., 2012). In comparing sites, we primarily focused on their relative stratigraphic trends and direction of nitrogen-cycle responses during the PETM. The compiled records reveal pronounced spatial and temporal heterogeneity in their stratigraphic $\delta^{15}N$ responses. With the exception of Site 865, marine records show varying degrees of $\delta^{15}N_{foram}$ decline or negative excursion during the PETM (Figs. 4 and 5; Khozyem et al., 2013, 2015; Junium et al., 2018a; Moretti et al., 2024; Yao et al., 2024). This widespread decline may reflect a decrease in the mean $\delta^{15}N_{nitrate}$ of the oceanic pycnocline nitrate reservoir, driven by a reorganization of the global fixed-nitrogen budget. Specifically, a reduced water-column denitrification compared to sedimentary denitrification could lower mean oceanic $\delta^{15}N_{nitrate}$ due to the former's larger isotope effect (Stüeken et al., 2016, 2024). At high-latitude Southern Ocean Site 690, where surface-water nutrient utilization was likely incomplete, the observed $\delta^{15}N_{foram}$ decline may partly reflect a decrease in pycnocline $\delta^{15}N_{nitrate}$ (Moretti et al., 2024). Basin-scale signals can be modified in various ways, by regional nutrient supply, nitrate utilization, ODZ dynamics, or the dominant form of bioavailable nitrogen, resulting in five distinct modes and settings described below.

5.3.2.1. Open-ocean nitrate-type systems. In open-ocean settings, upper-ocean $\delta^{15}N_{nitrate}$ compositions recorded by $\delta^{15}N_{foram}$ generally display the most positive background values, commonly exceeding 10‰. Their evolution during the PETM, however, differed markedly among regions. ODP Sites 1209 and 1210, located near the margin of the oligotrophic gyre in the tropical North Pacific, show an abrupt decrease in $\delta^{15}N_{foram}$ from ~+16‰ to +4‰ at the PETM onset, followed by a gradual recovery toward pre-event values (Fig. 4F; Moretti et al., 2024). Shell-size analysis of planktic and benthic foraminifera further indicates divergent oxygenation trends during the early PETM, with larger *Morozovella* suggesting enhanced tropical upper-ocean oxygenation and smaller benthic foraminifera indicating deep-ocean deoxygenation. This pattern is interpreted as reflecting a contraction of the upwelling-driven nutrient tongue, a band of nutrient-rich surface waters sustained by equatorial upwelling and extending from the eastern equatorial Pacific under PETM warming, which lowered export productivity and decreased O_2 consumption by organic matter remineralization in the shallow-subsurface ocean (Moretti et al., 2024). The resulting reduction in oxygen demand would have contracted nitrate-type ODZs, weakened water-column denitrification, and ultimately lowered $\delta^{15}N_{foram}$. The equatorial Pacific Site 865 where surface-nutrient dynamics were more directly influenced by high-productivity upwelling and the nutrient tongue exhibits a different response (Fig. 4G). The reversal of the $\delta^{15}N_{foram}$ relationship between Sites 865 and 1210 at the PETM onset is attributed to changes in nutrient-tongue extent and contrasting surface-nitrate utilization between the two regions. This indicates that, in upwelling systems, $\delta^{15}N_{foram}$ reflects not only ODZ intensity and water-column denitrification, but also the extent of nitrate consumption in surface waters.

5.3.2.2. Open-ocean ammonium-type systems. A different open-ocean pattern was reported by Yao et al. (2024) from South Atlantic ODP Sites 1263 and 1265 (Fig. 4H). These records show that $\delta^{15}N_{foram}$ decreased from ~+10‰ below the PETM to ~+4‰ during the event, followed by a rapid recovery to ~+9‰. At the same time, reactive phosphorus accumulation rates increased by factors between 4 and 9 in the PETM interval, an increase that coincided with a minimum in $\delta^{15}N_{foram}$ and a maximum in marine barite accumulation rate, indicating enhanced rather than reduced productivity. Yao et al. (2024) argued that the South Atlantic $\delta^{15}N_{foram}$ decline reflected the expansion of thermocline oxygen deficiency from suboxia to anoxia and the development of ammonium-type ODZs. This view is supported by marine barite $\delta^{34}S_{barite}$ records from Sites 1263 and 1265, which document a positive sulfur-isotope excursion consistent with a widespread expansion of anoxic and sulfidic waters during the PETM (Yao et al., 2018). Under such conditions, nitrate would have been extensively consumed and NH_4^+ accumulated in oxygen-deficient waters. When NH_4^+ was transported upward into the photic zone or into the upper chemocline, nitrification-coupled anammox and denitrification could have removed

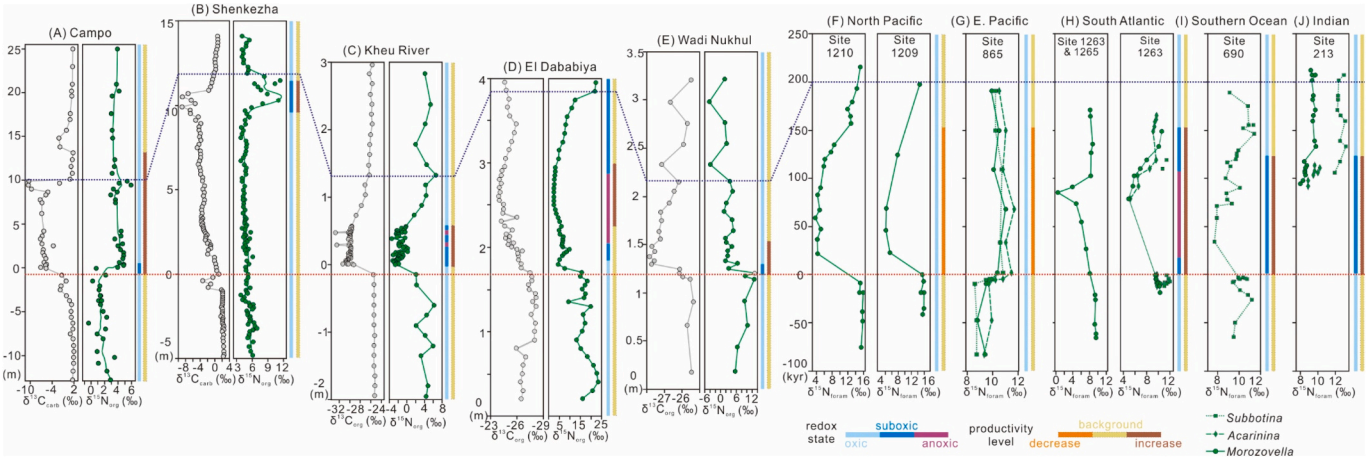


Fig. 4. Global correlation of nitrogen-isotope records during the PETM interval for localities shown in Fig. 1: Campo and Shenkezha (A-B; this study), Kheu River (C; Junium et al., 2018a), El Dababiya (D; Khozyem et al., 2015), Wadi Nukhul (E; Khozyem et al., 2013), North Pacific (F; Sites 1209 and 1210), Equator Pacific (G; Site 865), South Atlantic (H; Site 1263 from Moretti et al., 2024; composite Site 1263/1265 from Yao et al., 2024), Southern Ocean (I; Site 690) and Indian Ocean (J; Site 213; Moretti et al., 2024). Interpreted redox conditions and productivity levels are shown. Red and blue dotted lines represent PETM onset and end, respectively. (For interpretation of the references to colour in this figure legend, the reader is referred to the web version of this article.)

fixed nitrogen with a relatively weak net isotopic fractionation, thereby lowering $\delta^{15}N_{foram}$. Yao et al. (2024) emphasized that, to compensate for this intensified fixed-nitrogen loss, N_2 fixation must have increased by ~4.7 times relative to the pre-PETM rate, consistently with the productivity increase indicated by reactive phosphorus and marine barite records.

5.3.2.3. Restricted basins. The Kheu River section in the Peri-Tethys represents a restricted marine basin with a ~ 200 m maximum water depth (Junium et al., 2018a). During the PETM, calcareous mud was replaced by organic-rich sapropel with TOC contents of 2–9% and Fe-speciation evidence for oxygen-deficient to locally euxinic conditions. The $\delta^{15}N_{org}$ declined from a pre-PETM average of ~+3.8‰ to ~−1.7‰, with minima as low as −3.4‰, *i.e.*, too low to be explained solely by enhanced N_2 fixation (Fig. 4C). Junium et al. (2018a) ascribed this signal to PETM transgression, intensified hydrological cycling and freshwater input, which promoted estuarine-like circulation, nutrient retention, productivity, water-column stratification, and chemocline shoaling. NH_4^+ accumulated in anoxic to sulfidic deep waters and then mixed into the euphotic zone for phytoplankton assimilation, while NO_2^- and NO_3^- near the chemocline were removed by denitrification and anammox, thus explaining the negative $\delta^{15}N_{org}$ values of the sapropel.

5.3.2.4. Tethyan marginal-marine basins. Along the southern Tethyan margin of northeastern Africa, the upper-bathyal Wadi Nukhul section (~500 m water depth) and the outer-shelf El Dababiya section (~150–200 m water depth) record broadly similar PETM nitrogen-cycle perturbations (Khozyem et al., 2013, 2015). At Wadi Nukhul, the Paleocene–Eocene boundary is here represented by a 10-cm-thick clay-rich layer in which $\delta^{15}N_{org}$ abruptly decreases, remaining close to 0‰ above the boundary (Fig. 4E). This interval is characterized by a marked increase in P concentration and kaolinite percentage, abundant framboidal pyrite, and sedimentary structures related to cyanobacterial and sulfate-reducing bacterial activity, consistent with enhanced runoff, nutrient delivery, productivity, and organic-matter remineralization. The resulting oxygen consumption locally promoted dysoxic to anoxic conditions, while low N:P conditions favored N_2-fixing cyanobacteria, driving sedimentary $\delta^{15}N_{org}$ toward 0‰ or even negative values (Khozyem et al., 2013). In contrast, the more comprehensive El Dababiya succession records a more gradual decline in $\delta^{15}N_{org}$ from relatively high pre-PETM values to ~+2‰ during the main anoxic interval, followed by a progressive recovery (Fig. 4D). The lowest $\delta^{15}N_{org}$ values coincide with enhanced N_2-fixing bacterial organic-matter contributions and oxygen-deficient conditions, whereas the subsequent recovery has been linked to renewed nitrification and improved oxygenation (Khozyem et al., 2015). Overall, the two Egyptian sections indicate a broadly coherent regional shift toward enhanced microbial nitrogen cycling and N_2 fixation during the PETM.

5.3.2.5. Carbonate platforms. The compiled records discussed above indicate that marine nitrogen cycling was highly heterogeneous during the PETM event and cannot be explained by a single global mechanism (Figs. 4 and 5). In contrast with open-ocean, marginal and restricted Tethyan settings, the Campo and Shenkezha shallow-platform records lack pronounced and sustained negative $\delta^{15}N_{org}$ excursions. Campo shows a gradual positive shift, whereas Shenkezha exhibits relatively stable to slightly declining $\delta^{15}N_{org}$ through the main PETM interval followed by a pronounced positive excursion during recovery. The persistently positive $\delta^{15}N_{org}$ values argue against a dominant contribution from N_2 fixation or ammonium-based nitrogen cycling (Stüeken et al., 2016, 2024), which is ascribed to wave- and storm-driven mixing in these shallow-marine settings, inhibiting the development of persistent water-column stratification and anoxia (Li et al., 2020). Nitrate likely remained as a crucial source of bioavailable nitrogen, and the observed $\delta^{15}N_{org}$ variations probably integrated changes in the isotopic composition of source nitrate, the degree of nitrate utilization, and denitrification at the sediment–water interface. These platform records suggest that well-circulated shallow-marine environments were comparatively insulated from the extreme nitrogen-cycle states developed in open-ocean ODZs and strongly restricted basins, while remaining sensitive to changes in regional hydrologic cycle, nutrient transport, productivity, sea level, and regional redox state (Stüeken et al., 2016, 2024; Carmichael et al., 2017; Bridgestock et al., 2019).

Modern shelf environments provide a partial process-based analogue for this behavior. In shallow, hydrodynamically open settings, mixing driven by tides, wave, and wind can enhance water-column ventilation and limit the persistence of strong density stratification. In surface sediments, oxygen penetration promotes the nitrification of remineralized NH_4^+, whereas the resulting NO_3^- may either be returned to the overlying water or consumed by denitrification in adjacent anoxic microenvironments and deeper sedimentary layers. Modern observations and incubation experiments demonstrate active nitrate exchange, nitrification, and coupled nitrification–denitrification in shallow and permeable shelf sediments (Simon, 1988; Cheung et al., 2024). Together

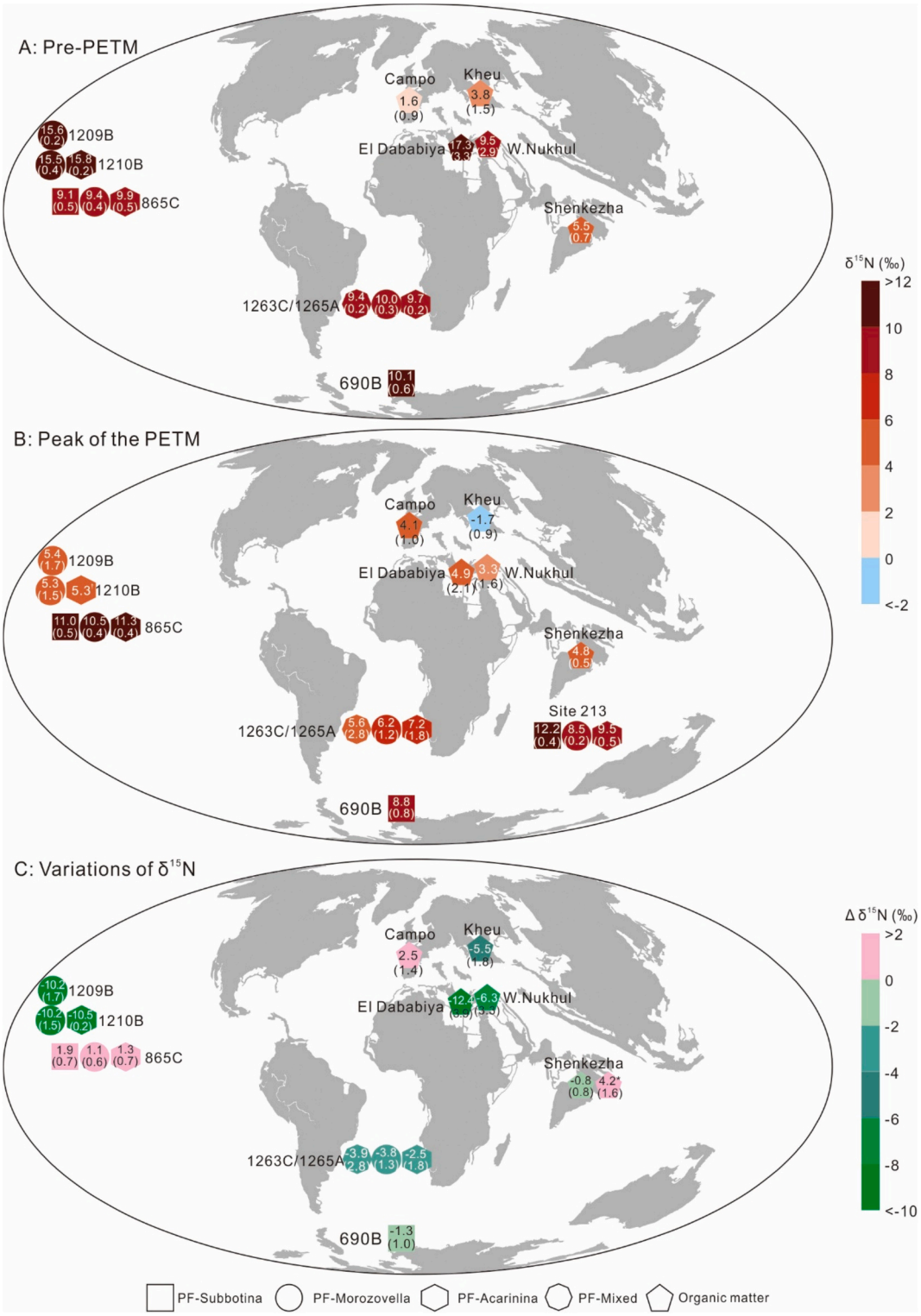


Fig. 5. Global comparison of nitrogen-isotope records during the PETM event. (A) Pre-PETM mean $\delta^{15}N$ (‰) values; (B) mean $\delta^{15}N$ (‰) values during PETM peak (within CIE body); (C) Variations of $\delta^{15}N$ (‰) between pre-PETM and PETM peak in each record. Numbers in parentheses represent standard deviation (SD). For Shenkezha section, asterisk represents $\delta^{15}N$ (‰) changes between means of PETM peak and recovery intervals. † indicates that only a single valid measure was available (Site 1210B in panel B). Data are plotted on Early Eocene paleogeographic maps (modified from Scotese, 2021). PF, planktonic foraminifera; Data sources as in Fig. 4.

with lateral water exchange, these processes could have limited persistent NH_4^+ accumulation and favored the maintenance of nitrate-based nitrogen cycling in well-ventilated shallow-marine settings, although their net effect on the fixed-nitrogen inventory depends on the balance among nutrient input, internal recycling, and nitrogen loss within sediments (Rippeth et al., 2024).

The Campo and Shenkezha records suggest that well-circulated carbonate platforms buffered regional nitrogen-cycle perturbations

during the PETM by maintaining nitrate-supported productivity and relatively oxygenated ecological niches, rather than by quantitatively compensating for global fixed-nitrogen loss. The strongly negative $\delta^{15}N_{org}$ response at the restricted Kheu River site indicates that such buffering depended on hydrodynamic openness and effective ventilation rather than on shallow water depth alone (Junium et al., 2018a). The PETM ocean thus likely comprised a spatial mosaic in which nitrate-type ODZs, ammonium-rich anoxic basins, N_2-fixation-dominated margins, and well-ventilated nitrate-supported platforms coexisted (Khozyem et al., 2013, 2015; Moretti et al., 2024; Yao et al., 2024). Shallow-water carbonate platforms may have consequently served as a safe house for nitrate-based marine ecosystems during a period of widespread nitrogen-cycle disruption.

5.4. *Implications for ocean biogeochemistry*

The compiled nitrogen-isotope records indicate that the PETM nitrogen cycle was strongly perturbed, but without evolving into a globally widespread OAE-like or mass-extinction-type nitrogen cycle (Figs. 5 and 6). During Mesozoic OAEs, enhanced productivity, widespread organic-rich black shale deposition, expansion of anoxic to euxinic waters, nitrate depletion, ammonium accumulation, and intensified N_2 fixation commonly produced low to negative $\delta^{15}N$ values over broad marine regions (Junium and Arthur, 2007, Junium et al., 2018b; Naafs et al., 2019; Zhai et al., 2023). Similar ammonium-dominated nitrogen cycling with low $\delta^{15}N$ values has been documented in poorly ventilated Late Cretaceous restricted-ocean settings (Du et al., 2025). At the Permian-Triassic boundary and during the Early Triassic hyperthermal, nitrogen isotopes displayed low values or a negative shift, reflecting an increased role of diazotrophy in response to nitrogen limitation in the photic zone and enhanced ammonium cycling under poorly ventilated conditions (Luo et al., 2011; Knies et al., 2013; Algeo et al., 2014; Du et al., 2021, 2024). During the PETM, some regions showed a similar behavior. The Kheu River sapropel and the South Atlantic ODP sites document NH_4^+ accumulation and nitrification-coupled anammox/denitrification, which resemble OAE-like nitrogen cycling especially where nitrate was depleted and ammonium became an important fixed-nitrogen reservoir (Figs. 5 and 6; Junium et al., 2018a; Yao et al., 2024). The southern Tethyan margin experienced marked N_2 fixation under low N:P conditions, driving sedimentary $\delta^{15}N_{org}$ toward extremely low values, which resemble PTB-like nitrogen cycling (Khozyem et al., 2013, 2015). The tropical North Pacific recorded a contraction of nitrate-type ODZs and weakened water-column denitrification, whereas the Campo and Shenkezha sections exhibit stable to elevated $\delta^{15}N_{org}$ values best explained by nitrate-based cycling, enhanced nitrate utilization, and local or sediment-water interface denitrification (Figs. 5 and 6; Moretti et al., 2024). This contrast suggests that the PETM ocean was not a simple analogue of Mesozoic OAEs or major mass-extinction events, but rather a spatial mosaic of nitrogen-cycle states controlled by regional oxygenation, productivity, circulation, and depositional setting.

The Campo and Shenkezha records further imply that shallow-marine carbonate platforms acted as local nitrogen-cycle reactors rather than passive recorders of a global marine $\delta^{15}N$ signal during the PETM. In these settings, intensified hydrological cycling and terrestrial nutrient delivery could stimulate productivity and organic-matter remineralization, but the isotopic response depended on whether oxygen deficiency developed in the water column, near the sediment-water interface, or mainly within pore waters. At Campo, enhanced runoff likely increased nutrient and nitrate supply, thereby sustaining local denitrification and the development of a ^{15}N-enriched bioavailable nitrogen pool (Li et al., 2021). At Shenkezha, the PETM core interval

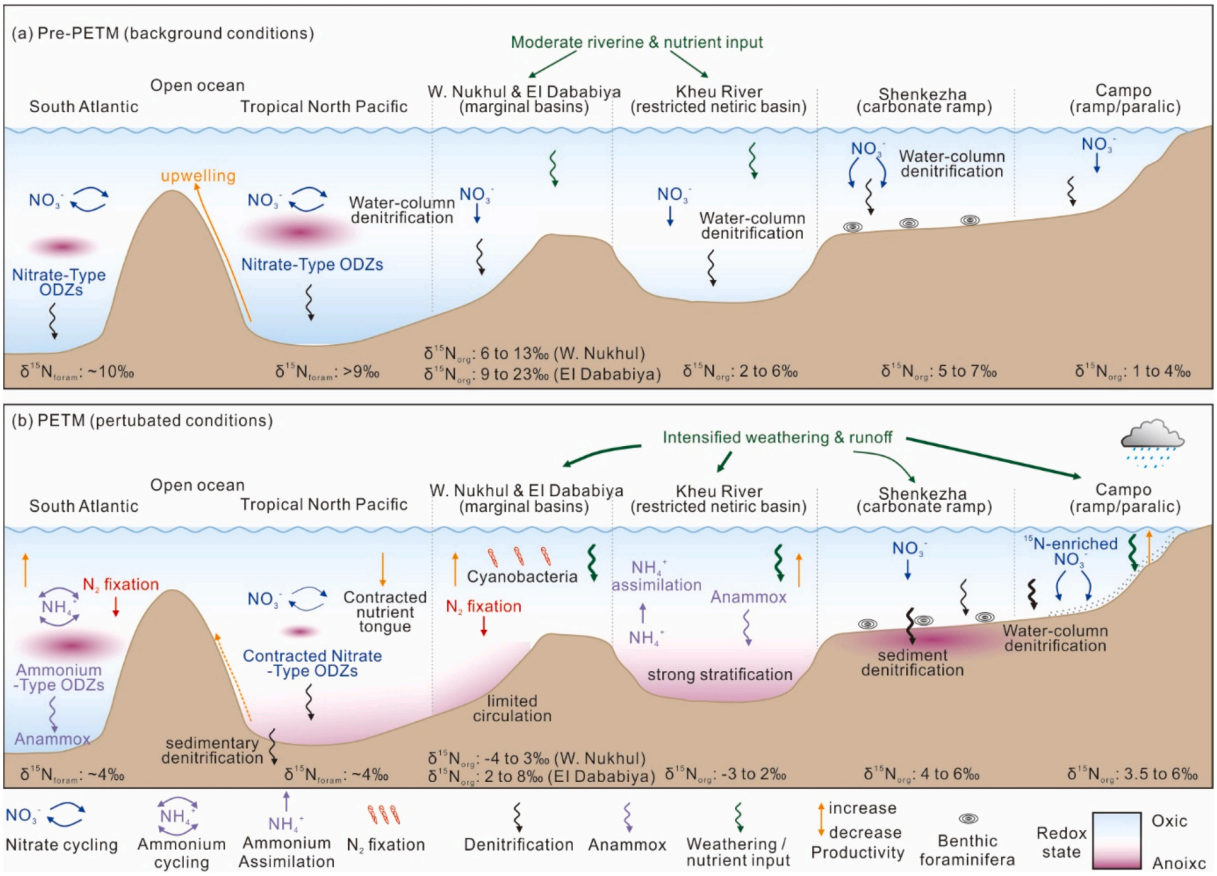


Fig. 6. Schematic evolution of climate and environment during the PETM and envisaged impact on marine nitrogen cycling.

appears to have remained largely nitrate-based, with reducing conditions mostly restricted to pore waters, whereas regression and transient suboxia during the PETM recovery may have enhanced local denitrification and generated the positive $\delta^{15}N_{org}$ excursion (Li et al., 2020; Zhang et al., 2023). These observations suggest that shallow-platform nitrogen cycling could regulate local nutrient availability through sedimentary fixed-nitrogen removal, potentially limiting productivity where nitrogen loss exceeded external supply and internal recycling, but sustaining or enhancing productivity where nutrient replenishment was sufficient to offset this loss (Cheung et al., 2024).

Importantly, shallow-marine nitrogen cycling during the PETM may have implications for marine N_2O cycling, although this remains a mechanistic possibility. Denitrification and nitrification can both produce N_2O under low-oxygen conditions, and modern ODZs are important sites of marine N_2O cycling (Ji et al., 2015; Bange et al., 2019). N_2O is climatically important because of its strong greenhouse effect, ~273 times that of CO_2 (IPCC, 2021). By analogy with modern low-oxygen environments, transient deoxygenation in shallow platforms and marginal basins during the PETM could have favored N_2O production through incomplete denitrification or coupled nitrification-denitrification (Babbin et al., 2015; Frey et al., 2020). The magnitude of the N_2O flux, however, cannot be assessed from the available records. Such a mechanism would be most plausible in redox-transition zones. In intermittently oxygenated settings, nitrification, nitrate reduction, and incomplete denitrification can coexist and promote N_2O production (Naqvi et al., 2010; Ji et al., 2015; Frey et al., 2020). In persistently anoxic or euxinic settings, instead, denitrification may proceed more completely to N_2, and anammox can remove fixed nitrogen without necessarily producing large N_2O fluxes (Canfield et al., 2010; Babbin et al., 2015). Accordingly, shallow chemoclines, fluctuating sediment-water interfaces, and intermittently suboxic platform waters may have provided favorable conditions for episodic N_2O production (Naqvi et al., 2010; Babbin et al., 2015; Frey et al., 2020). The Campo and Shenkezha sections are relevant in this context because they document carbonate-platform records where redox conditions may have fluctuated between oxic, suboxic, and reducing pore-water states. Such environments may have acted as localized but widespread biogeochemical interfaces, modulating fixed-nitrogen loss, N_2O production potential, and nutrient feedbacks during PETM warming (Naqvi et al., 2010; Frey et al., 2020; Stüeken et al., 2024).

Nitrogen cycling during the PETM was characterized by strong spatial heterogeneity. Restricted marginal basins and some open-ocean thermocline settings approached ammonium-rich, OAE-like nitrogen cycling, but shallow-marine carbonate platforms largely retained nitrate-based cycling and responded through local nitrate utilization and denitrification. This distinction is important because it suggests that shallow-marine systems could both buffer and amplify PETM climate perturbations: they may buffer productivity by promoting fixed-nitrogen loss as well as amplify greenhouse effects through episodic N_2O production under fluctuating low-oxygen conditions.

The PETM event provides an example of how rapid greenhouse warming can reorganize marine nitrogen cycling into multiple regional modes, with varied consequences for ocean chemistry, productivity, and climate feedbacks. Similar spatial heterogeneity in marine nitrogen cycling has been documented during other greenhouse crises such as the end-Triassic interval, when near-zero or negative $\delta^{15}N_{org}$ shifts characterized the Panthalassan Ocean, whereas the Central European Basin recorded relatively less negative or positive $\delta^{15}N_{org}$ values (Li et al., 2025). Overall, this suggests that spatially heterogeneous nitrogen cycling was a common phenomenon during deep-time greenhouse perturbations.

6. Conclusions

This study provides new nitrogen-isotope records from the Campo and Shenkezha shallow-marine carbonate successions in Spain and southern Tibet, offering insight into nitrogen cycling on carbonate platforms during the PETM. Both sections record relatively stable to elevated $\delta^{15}N_{org}$ values rather than the pronounced negative excursions observed in several open-ocean, restricted-basin, and marginal-basin records, indicating that carbonate platforms recorded different nitrogen-cycling processes. At Campo, elevated $\delta^{15}N_{org}$ values are associated with enhanced nutrient supply, increased productivity, and potential mild water-column deoxygenation, suggesting that local nitrate utilization and denitrification enriched the bioavailable nitrogen pool in ^{15}N. At Shenkezha, stable $\delta^{15}N_{org}$ values in the PETM core interval and a positive excursion during the recovery stage indicate a two-step response, with pore-water anoxia followed by enhanced sediment-water interface redox fluctuations and local denitrification.

A comparison with published PETM records demonstrates that marine nitrogen cycling was spatially highly heterogeneous. Negative nitrogen-isotope excursions in different settings may reflect contraction of nitrate-type ODZs, enhanced N_2 fixation, or ammonium-rich cycling and assimilation, whereas the Campo and Shenkezha records define a shallow-platform mode dominated by nitrate-based cycling, local nitrate utilization, and water-column or sedimentary denitrification. These results highlight the sensitivity of shallow-marine nitrogen cycling to hydrological change, terrestrial nutrient delivery, and local redox structure during rapid greenhouse warming.

CRediT authorship contribution statement

Jingxin Jiang: Writing – review & editing, Writing – original draft, Visualization, Methodology, Formal analysis. **Xiumian Hu:** Writing – review & editing, Funding acquisition, Conceptualization. **Zhong Han:** Writing – review & editing. **Thomas J. Algeo:** Writing – review & editing. **Xi Chen:** Writing – review & editing. **Eduardo Garzanti:** Writing – review & editing.

Declaration of competing interest

The authors declare that they have no known competing financial interests or personal relationships that could have appeared to influence the work reported in this paper.

Acknowledgments

We sincerely thank Dr. Weiqi Yao and an anonymous reviewer for their thoughtful and constructive comments, which significantly improved the clarity and quality of our manuscript. We dedicate this paper to the memory of our dear friend Dr. Juan Li, whose passion and commitment will always be remembered. This study, completed on the foundation of Dr. Li Juan's earlier work, was supported by the National Key Research and Development Program of China (grant 2023YFF0804000), National Natural Science Foundation of China (42402126, 42488201, 42072117), China Postdoctoral Science Foundation (2024M751379), and Postdoctoral Fellowship Program of China Postdoctoral Science Foundation (GZC20231096). This is a contribution to IGCP739.

Appendix A. Supplementary data

Supplementary data to this article can be found online at https://doi.org/10.1016/j.gloplacha.2026.105791.

Data availability

The authors confirm that all data necessary for supporting the scientific findings of this paper have been provided.

References

Ader, M., Sansjofre, P., Halverson, G.P., Busigny, V., Trindade, R.I.F., Kunzmann, M., Nogueira, A.C.R., 2014. Ocean redox structure across the Late Neoproterozoic Oxygenation Event: a nitrogen isotope perspective. Earth Planet. Sci. Lett. 396, 1–13.

Algeo, T., Rowe, H., Hower, J.C., Schwark, L., Herrmann, A., Heckel, P., 2008. Changes in ocean denitrification during late Carboniferous glacial–interglacial cycles. Nat. Geosci. 1 (10), 709–714.

Algeo, T.J., Meyers, P.A., Robinson, R.S., Rowe, H., Jiang, G.Q., 2014. Icehouse–greenhouse variations in marine denitrification. Biogeosciences 11 (4), 1273–1295.

Altabet, M.A., Francois, R., Murray, D.W., Prell, W.L., 1995. Climate-related variations in denitrification in the Arabian Sea from sediment $^{15}N/^{14}N$ ratios. Nature 373 (6514), 506–509.

Aze, T., Pearson, P.N., Dickson, A.J., Badger, M.P., Bown, P.R., Pancost, R.D., Gibbs, S.J., Huber, B.T., Leng, M.J., Coe, A.L., Cohen, A.S., Foster, G.L., 2014. Extreme warming of tropical waters during the Paleocene–Eocene thermal maximum. Geology 42 (9), 739–742.

Babbin, A.R., Bianchi, D., Jayakumar, A., Ward, B.B., 2015. Rapid nitrous oxide cycling in the suboxic ocean. Science 348, 1127–1129.

Bange, H.W., Sim, C.H., Bastian, D., Kallert, J., Kock, A., Mujahid, A., Müller, M., 2019. Nitrous oxide (N_2O) and methane (CH_4) in rivers and estuaries of northwestern Borneo. Biogeosciences 16 (22), 4321–4335.

Brandes, J.A., Devol, A.H., 2002. A global marine-fixed nitrogen isotopic budget: implications for Holocene nitrogen cycling. Glob. Biogeochem. Cycles 16 (4), 67–1.

Bridgestock, L., Hsieh, Y.T., Porcelli, D., Henderson, G.M., 2019. Increased export production during recovery from the Paleocene–Eocene thermal maximum constrained by sedimentary Ba isotopes. Earth Planet. Sci. Lett. 510, 53–63.

Canfield, D.E., Glazer, A.N., Falkowski, P.G., 2010. The evolution and future of Earth's nitrogen cycle. Science 330, 192–196.

Carmichael, M.J., Inglis, G.N., Badger, M.P., Naafs, B.D., Behrooz, L., Remmelzwaal, S., Monteiro, F.M., Rohrssen, M., Farnsworth, A., Buss, H.L., 2017. Hydrological and associated biogeochemical consequences of rapid global warming during the Paleocene-Eocene thermal maximum. Glob. Planet. Change 157, 114–138.

Casciotti, K.L., 2009. Inverse kinetic isotope fractionation during bacterial nitrite oxidation. Geochim. Cosmochim. Acta 73 (7), 2061–2076.

Casciotti, K.L., Sigman, D.M., Ward, B.B., 2003. Linking diversity and stable isotope fractionation in ammonia-oxidizing bacteria. Geomicrobiol J. 20 (4), 335–353.

Chang, C., Algeo, T.J., 2025. Nitrogen cycling and marine redox evolution during the Ediacaran–Cambrian transition. Glob. Planet. Change 245, 104679.

Cheung, H.L.S., Hillman, J.R., Pilditch, C.A., Savage, C., Santos, I.R., Glud, R.N., Nascimento, F.J.A., Thrush, S.F., Bonaglia, S., 2024. Denitrification, anammox, and DNRA in oligotrophic continental shelf sediments. Limnol. Oceanogr. 69, 621–637.

Clarkson, M.O., Lenton, T.M., Andersen, M.B., Bagard, M.L., Dickson, A.J., Vance, D., 2021. Upper limits on the extent of seafloor anoxia during the PETM from uranium isotopes. Nat. Commun. 12 (1), 399.

Dodd, M.S., Zhang, Z., Li, C., Algeo, T.J., Lyons, T.W., Hardisty, D.S., Loyd, S.J., Meyer, D.L., Gill, B.C., Shi, W., Wang, W., 2021. Development of carbonate-associated phosphate (CAP) as a proxy for reconstructing ancient ocean phosphate levels. Geochim. Cosmochim. Acta 301, 48–69.

Du, Y., Song, H., Algeo, T.J., Zhang, H., Peng, J., Wu, Y., Lai, J., Shu, X., Song, H., Wei, L., Zhang, J., Stüeken, E.E., Grasby, S.E., Dal Corso, J., Liu, X., Chu, D., Tian, L., Liang, Q., Li, X., Yao, H., Song, H., 2026. The global Deep-time Sediment Nitrogen Isotopes in Marine Systems (DSMS-NI) database. Earth Syst. Sci. Data 18, 675–690.

Du, Y., Song, H., Algeo, T.J., Zhong, L., Li, J., Song, H., 2025. Tectonic controls on nitrogen cycling and ocean ventilation dynamics in the Late Cretaceous equatorial Atlantic. Earth Planet. Sci. Lett. 667, 119517.

Du, Y., Song, H., Stüeken, E.E., Grasby, S.E., Song, H., Tian, L., Chu, D., Dal Corso, J., Li, Z., Tong, J., 2024. Large nitrogen cycle perturbations during the Early Triassic hyperthermal. Geochim. Cosmochim. Acta 382, 13–25.

Du, Y., Song, H., Tong, J., Algeo, T.J., Li, Z., Song, H., Huang, J., 2021. Changes in productivity associated with algal-microbial shifts during the Early Triassic recovery of marine ecosystems. Bulletin 133 (1–2), 362–378.

Dymond, J., Suess, E., Lyle, M., 1992. Barium in deep-sea sediment: a geochemical proxy for paleoproductivity. Paleoceanography 7 (2), 163–181.

Frey, C., Bange, H.W., Achterberg, E.P., et al., 2020. Regulation of nitrous oxide production in low-oxygen waters off the coast of Peru. Biogeosciences 17, 2263–2287.

Fujisaki, W., Sawaki, Y., Matsui, Y., Yamamoto, S., Isozaki, Y., Maruyama, S., 2019. Redox condition and nitrogen cycle in the Permian deep mid-ocean: a possible contrast between Panthalassa and Tethys. Glob. Planet. Change 172, 179–199.

Füssel, J., Lam, P., Lavik, G., Jensen, M.M., Holtappels, M., Günter, M., Kuypers, M.M., 2012. Nitrite oxidation in the Namibian oxygen minimum zone. ISME J. 6 (6), 1200–1209.

Garzanti, E., 2026. The stratigraphy of the Tethys Himalaya. Ital. J. Geosci. 145 (1), 74–96.

Geider, R.J., La Roche, J., 2002. Redfield revisited: variability of C [ratio] N [ratio] P in marine microalgae and its biochemical basis. Eur. J. Phycol. 37 (1), 1–17.

Gonneea, M.E., Paytan, A., 2006. Phase associations of barium in marine sediments. Mar. Chem. 100 (1–2), 124–135.

Gruber, N., Sarmiento, J.L., 1997. Global patterns of marine nitrogen fixation and denitrification. Global Biogeochem. Cycles 11 (2), 235–266.

Hu, X.M., Sinclair, H.D., Wang, J.G., Jiang, H., Wu, F.Y., 2012. Late Cretaceous-Palaeogene stratigraphic and basin evolution in the Zhepure Mountain of southern Tibet: implications for the timing of India-Asia initial collision. Basin Res. 24 (5), 520–543.

Hunt, D., Tucker, M.E., 1992. Stranded parasequences and the forced regressive wedge systems tract: deposition during base-level fall. Sediment. Geol. 81 (1–2), 1–9.

Hutchins, D.A., Capone, D.G., 2022. The marine nitrogen cycle: new developments and global change. Nat. Rev. Microbiol. 20 (7), 401–414.

IPCC, 2021. Climate Change 2021: The Physical Science Basis. Contribution of Working Group I to the Sixth Assessment Report of the Intergovernmental Panel on Climate Change.

Jenkyns, H.C., Gröcke, D.R., Hesselbo, S.P., 2001. Nitrogen isotope evidence for water mass denitrification during the early Toarcian (Jurassic) oceanic anoxic event. Paleoceanography 16 (6), 593–603.

Ji, Q., Babbin, A.R., Jayakumar, A., Oleynik, S., Ward, B.B., 2015. Nitrous oxide production by nitrification and denitrification in the Eastern Tropical South Pacific oxygen minimum zone. Geophys. Res. Lett. 42 (24), 10–755.

Jiang, J., Hu, X., Garzanti, E., Cui, Y., Algeo, T.J., 2026. Millennial-scale changes in marine lithofacies during the Paleocene-Eocene Thermal Maximum: a deep-time analog for Anthropocene hydrologic and acidification impacts. Earth Sci. Rev. 277, 105474.

Jin, S., Li, G., Li, J., Hu, X., Yang, H., Huang, C., Baoke, Z., Algeo, T.J., Kemp, D.B., 2023. Tropical ocean temperatures and changes in terrigenous flux during the Paleocene-Eocene thermal maximum in southern Tibet. Glob. Planet. Change 230, 104289.

Junium, C.K., Arthur, M.A., 2007. Nitrogen cycling during the Cretaceous, Cenomanian-Turonian oceanic anoxic event II. Geochem. Geophys. Geosyst. 8 (3), 1–18.

Junium, C.K., Dickson, A.J., Uveges, B.T., 2018a. Perturbation to the nitrogen cycle during rapid Early Eocene global warming. Nat. Commun. 9 (1), 3186.

Junium, C.K., Meyers, S.R., Arthur, M.A., 2018b. Nitrogen cycle dynamics in the Late Cretaceous Greenhouse. Earth Planet. Sci. Lett. 481, 404–411.

Kalvelage, T., Lavik, G., Lam, P., Contreras, S., Arteaga, L., Löscher, C.R., Oschlies, A., Paulmier, A., Stramma, L., Kuypers, M.M., 2013. Nitrogen cycling driven by organic matter export in the South Pacific oxygen minimum zone. Nat. Geosci. 6 (3), 228–234.

Kennett, J.P., Stott, L.D., 1991. Abrupt deep-sea warming, palaeoceanographic changes and benthic extinctions at the end of the Palaeocene. Nature 353 (6341), 225–229.

Khozyem, H., Adatte, T., Spangenberg, J.E., Keller, G., Tantawy, A.A., Ulianov, A., 2015. New geochemical constraints on the Paleocene–Eocene thermal maximum: Dababiya GSSP, Egypt. Palaeogeogr. Palaeoclimatol. Palaeoecol. 429, 117–135.

Khozyem, H., Adatte, T., Spangenberg, J.E., Tantawy, A.A., Keller, G., 2013. Palaeoenvironmental and climatic changes during the Palaeocene–Eocene thermal maximum (PETM) at the Wadi Nukhul section, Sinai, Egypt. J. Geol. Soc. 170 (2), 341–352.

Knies, J., Grasby, S.E., Beauchamp, B., Schubert, C.J., 2013. Water mass denitrification during the latest Permian extinction in the Sverdrup Basin, Arctic Canada. Geology 41 (2), 167–170.

Lawrence, M.G., Greig, A., Collerson, K.D., Kamber, B.S., 2006. Rare earth element and yttrium variability in South East Queensland waterways. Aquat. Geochem. 12 (1), 39–72.

Li, C., Jian, Z., Jia, G., Dang, H., Wang, J., 2019. Nitrogen fixation changes regulated by upper water structure in the South China Sea during the last two glacial cycles. Global Biogeochem. Cycles 33 (8), 1010–1025.

Li, J., Hu, X.M., Garzanti, E., An, W., Wang, J.G., 2015. Paleogene carbonate microfacies and sandstone provenance (Gamba area, South Tibet): stratigraphic response to initial India-Asia continental collision. J. Asian Earth Sci. 104, 39–54.

Li, J., Hu, X.M., Garzanti, E., BouDagher-Fadel, M., 2021. Climate-driven hydrological change and carbonate platform demise induced by the Paleocene–Eocene Thermal Maximum (southern Pyrenees). Palaeogeography Palaeoclimatology Palaeoecology 567, 110250.

Li, J., Hu, X.M., Garzanti, E., BouDagher-Fadel, M., 2022. Spatial heterogeneity in carbonate-platform environments and carbon isotope values across the Paleocene–Eocene thermal maximum (Tethys Himalaya, South Tibet). Glob. Planet. Change 214, 103853.

Li, J., Hu, X.M., Zachos, J.C., Garzanti, E., BouDagher-Fadel, M., 2020. Sea level, biotic and carbon-isotope response to the Paleocene–Eocene thermal maximum in Tibetan Himalayan platform carbonates. Glob. Planet. Change 194, 103316.

Li, J., Song, H., Du, Y., Wignall, P.B., Bond, D.P.G., Grasby, S.E., Song, H., Dal Corso, J., Tian, L., Chu, D., 2025. Spatial and temporal heterogeneity of the marine nitrogen cycle during the end-Triassic mass extinction. Chem. Geol. 682, 122752.

Luo, G., Wang, Y., Algeo, T.J., Kump, L.R., Bai, X., Yang, H., Yao, L., Xie, S., 2011. Enhanced nitrogen fixation in the immediate aftermath of the latest Permian marine mass extinction. Geology 39 (7), 647–650.

Marconi, D., Weigand, M.A., Rafter, P.A., McIlvin, M.R., Forbes, M., Casciotti, K.L., Sigman, D.M., 2015. Nitrate isotope distributions on the US GEOTRACES North Atlantic cross-basin section: signals of polar nitrate sources and low latitude nitrogen cycling. Mar. Chem. 177, 143–156.

Martiny, A.C., Vrugt, J.A., Primeau, F.W., Lomas, M.W., 2013. Regional variation in the particulate organic carbon to nitrogen ratio in the surface ocean. Global Biogeochem. Cycles 27 (3), 723–731.

McInerney, F.A., Wing, S.L., 2011. The Paleocene-Eocene Thermal Maximum: a perturbation of carbon cycle, climate, and biosphere with implications for the future. Annu. Rev. Earth Planet. Sci. 39 (1), 489–516.

Meyers, P.A., 1997. Organic geochemical proxies of paleoceanographic, paleolimnologic, and paleoclimatic processes. Org. Geochem. 27 (5–6), 213–250.

Morel, F.M., Price, N.M., 2003. The biogeochemical cycles of trace metals in the oceans. Science 300 (5621), 944–947.

Moretti, S., Auderset, A., Deutsch, C., Schmitz, R., Gerber, L., Thomas, E., Luciani, V., Petrizzo, M.R., Schiebel, R., Tripati, A., Sexton, P., Norris, R., D'Onofrio, R., Zachos, J., Sigman, D.M., Haug, G.H., Martínez-García, A., 2024. Oxygen rise in the

tropical upper ocean during the Paleocene-Eocene thermal maximum. Science 383 (6684), 727–731.
Mulder, A., Van de Graaf, A.A., Robertson, L.A., Kuenen, J.G., 1995. Anaerobic ammonium oxidation discovered in a denitrifying fluidized bed reactor. FEMS Microbiol. Ecol. 16 (3), 177–183.
Murray, J.W., Fuchsman, C., Kirkpatric, J., Paul, B., Konovalov, S.K., 2005. Species and $\delta^{15}N$ signatures of nitrogen transformations in the suboxic zone of the Black Sea. Oceanography 18, 36–47.
Naafs, B.D.A., Monteiro, F.M., Pearson, A., Higgins, M.B., Pancost, R.D., Ridgwell, A., 2019. Fundamentally different global marine nitrogen cycling in response to severe ocean deoxygenation. Proceedings of the National Academy of Sciences (USA) 116 (50), 24979–24984.
Naqvi, S.W.A., Bange, H.W., Farías, L., Monteiro, P.M.S., Scranton, M.I., Zhang, J., 2010. Marine hypoxia/anoxia as a source of CH_4 and N_2O. Biogeosciences 7, 2159–2190.
Payros, A., Pujalte, V., Baceta, J.I., Bernaola, G., Orue-Etxebarria, X., Apellaniz, E., Caballero, F., Ferrandez, C., 2000. Lithostratigraphy and sequence stratigraphy of the upper Thanetian to middle Ilerdian strata of the Campo section, southern Pyrenees, Spain: revision and new data. Rev. Soc. Geol. Esp. 13 (2), 213–226.
Paytan, A., Averyt, K., Faul, K., Gray, E., Thomas, E., 2007. Barite accumulation, ocean productivity, and Sr/Ba in barite across the Paleocene–Eocene thermal maximum. Geology 35 (12), 1139–1142.
Plaziat, J.C., 1981. Late Cretaceous to late Eocene palaeogeographic evolution of southwest Europe. Palaeogeography Palaeoclimatology Palaeoecology 36, 263–320.
Pujalte, V., Schmitz, B., Baceta, J.I., 2014. Sea-level changes across the Paleocene Eocene interval in the Spanish Pyrenees, and their possible relationship with North Atlantic magmatism. Palaeogeography Palaeoclimatology Palaeoecology 393, 45–60.
Rafter, P.A., Bagnell, A., Marconi, D., DeVries, T., 2019. Global trends in marine nitrate N isotopes from observations and a neural network-based climatology. Biogeosciences 16 (13), 2617–2633.
Rafter, P.A., Sigman, D.M., Charles, C.D., Kaiser, J., Haug, G.H., 2012. Subsurface tropical Pacific nitrogen isotopic composition of nitrate: biogeochemical signals and their transport. Glob. Biogeochem. Cycles 26 (1), 1–14.
Ren, H., Sigman, D.M., Thunell, R.C., Prokopenko, M.G., 2012. Nitrogen isotopic composition of planktonic foraminifera from the modern ocean and recent sediments. Limnol. Oceanogr. 57 (4), 1011–1024.
Rippeth, T., Shen, S., Lincoln, B., Scannell, B., Meng, X., Hopkins, J., Sharples, J., 2024. The deepwater oxygen deficit in stratified shallow seas is mediated by diapycnal mixing. Nat. Commun. 15 (1), 3136.
Robinson, R.S., Kienast, M., Albuquerque, A.L., Altabet, M., Contreras, S., De Pol-Holz, R., Dubois, N., Francois, R., Galbraith, E., Hsu, T.C., Ivanochko, T., Jaccard, S., Kao, S.J., Kiefer, T., Kienast, S., Lehmann, M.F., Martinez, P., McCarthy, M., Möbius, J., Pedersen, T., Quan, T.M., Ryabenko, E., Schmittner, A., Schneider, R., Schneider-Mor, A., Shigemitsu, M., Sinclair, D., Somes, C., Studer, A., Thunell, R., Yang, J.Y., 2012. A review of nitrogen isotopic alteration in marine sediments. Paleoceanography 27, PA4203.
Roest, W.R., Srivastava, S.P., 1991. Kinematics of the plate boundaries between Eurasia, Iberia, and Africa in the North Atlantic from the late Cretaceous to the present. Geology 19, 613–616.
Scheibner, C., Rasser, M.W., Mutti, M., 2007. The Campo section (Pyrenees, Spain) revisited: implications for changing benthic carbonate assemblages across the Paleocene-Eocene boundary. Palaeogeography Palaeoclimatology Palaeoecology 248, 145–168.
Schoepfer, S.D., Shen, J., Wei, H., Tyson, R.V., Ingall, E., Algeo, T.J., 2015. Total organic carbon, organic phosphorus, and biogenic barium fluxes as proxies for paleomarine productivity. Earth-Science Reviews 149, 23–52.
Sciunnach, D., Garzanti, E., 2012. Subsidence history of the Tethys Himalaya. Earth-Sci. Rev. 25, 179–198.
Scotese, C.R., 2021. An atlas of Phanerozoic paleogeographic maps: the seas come in and the seas go out. Annu. Rev. Earth Planet. Sci. 49 (1), 679–728.
Sigman, D.M., Altabet, M.A., McCorkle, D.C., Francois, R., Fischer, G., 1999. The $\delta^{15}N$ of nitrate in the Southern Ocean: consumption of nitrate in surface waters. Global Biogeochem. Cycles 13 (4), 1149–1166.
Sigman, D.M., Karsh, K.L., Casciotti, K.L., 2009. Nitrogen isotopes in the ocean. In: Steele, J.H. (Ed.), Encyclopedia of Ocean Sciences, 3rd edn, pp. 40–54.
Simon, N.S., 1988. Nitrogen cycling between sediment and the shallow-water column in the transition zone of the Potomac River and estuary. I. Nitrate and ammonium fluxes. Estuar. Coast. Shelf Sci. 26 (5), 483–497.
Soliman, M.F., Aubry, M.P., Schmitz, B., Sherrell, R.M., 2011. Enhanced coastal paleoproductivity and nutrient supply in Upper Egypt during the Paleocene/Eocene Thermal Maximum (PETM): mineralogical and geochemical evidence. Palaeogeogr. Palaeoclimatol. Palaeoecol. 310 (3–4), 365–377.
Stüeken, E., Buick, R., Schauer, A.J., 2015. Nitrogen isotope evidence for alkaline lakes on late Archean continents. Earth Planet. Sci. Lett. 411, 1–10.
Stüeken, E.E., Kipp, M.A., Koehler, M.C., Buick, R., 2016. The evolution of Earth's biogeochemical nitrogen cycle. Earth-Science Reviews 160, 220–239.
Stüeken, E.E., Pellerin, A., Thomazo, C., Johnson, B.W., Duncanson, S., Schoepfer, S.D., 2024. Marine biogeochemical nitrogen cycling through Earth's history. Nat. Rev. Earth Environ. 5 (10), 732–747.
Sun, X., Fan, D., Hu, L., Wang, H., 2025. Global patterns and drivers of nitrogen isotope signal in modern marine sediments. Nat. Commun. 16 (1), 11363.
Taylor, S.R., McLennan, S.M., 1985. The Continental Crust: Its Composition and Evolution. Oxford Press, Blackwell, pp. 1–312.
Tesdal, J.E., Galbraith, E.D., Kienast, M., 2013. Nitrogen isotopes in bulk marine sediment: linking seafloor observations with subseafloor records. Biogeosciences 10 (1), 101–118.
Thunell, R.C., Sigman, D.M., Mulle-Karger, F., Astor, Y., Varela, R., 2004. Nitrogen isotope dynamics of the Cariaco Basin, Venezuela. Glob. Biogeochem. Cycles 18 (3).
Tierney, J.E., Zhu, J., Li, M., Ridgwell, A., Hakim, G.J., Poulsen, C.J., Whiteford, R., Rae, J.W., Kump, L.R., 2022. Spatial patterns of climate change across the Paleocene–Eocene thermal maximum. Proc. Natl. Acad. Sci. U. S. A. 119 (42), e2205326119.
Tostevin, R., Shields, G.A., Tarbuck, G.M., He, T., Clarkson, M.O., Wood, R.A., 2016. Effective use of cerium anomalies as a redox proxy in carbonate-dominated marine settings. Chem. Geol. 438, 146–162.
Tribovillard, N., Algeo, T.J., Lyons, T., Riboulleau, A., 2006. Trace metals as paleoredox and paleoproductivity proxies: An update. Chem. Geol. 232 (1–2), 12–32.
Wang, J.G., Hu, X.M., Jansa, L., Huang, Z.C., 2011. Provenance of the Upper Cretaceous-Eocene deep-water sandstones in Sangdanlin, Southern Tibet: constraints on the timing of initial India-Asia collision. J. Geol. 119, 293–309.
Wang, X.Q., Jiang, G.Q., Shi, X.Y., Peng, Y.B., Morales, D.C., 2018. Nitrogen isotope constraints on the early Ediacaran Ocean redox structure. Geochim. Cosmochim. Acta 240, 220–235.
Wang, X.T., Sigman, D.M., Cohen, A.L., Sinclair, D.J., Sherrell, R.M., Cobb, K.M., Erler, D.V., Stolarski, J., Kitahara, M.V., Ren, H., 2016. Influence of open ocean nitrogen supply on the skeletal $\delta^{15}N$ of modern shallow-water scleractinian corals. Earth Planet. Sci. Lett. 441, 125–132.
Xu, Y., Wang, C., Ji, K., Hong, H., Algeo, T.J., Christidis, G.E., Chenlei, Z., Lourens, L.J., Gingerich, P.D., Abels, H.A., 2025. Reduced mean annual precipitation immediately after the onset of the Paleocene-Eocene thermal maximum in the Bighorn Basin (Wyoming, USA). Palaeogeogr. Palaeoclimatol. Palaeoecol. 678, 113205.
Yang, S., Hu, W., Wang, X., Fan, J., 2021. Nitrogen isotope evidence for a redox-stratified ocean and eustasy-driven environmental evolution during the Ordovician–Silurian transition. Glob. Planet. Change 207, 103682.
Yao, W., Kong, T., Wang, X.T., Zhai, R., Zhang, R., Liu, Y., 2024. Expanded subsurface ocean anoxia in the Atlantic during the Paleocene-Eocene Thermal Maximum. Nat. Commun. 15 (1), 9053.
Yao, W., Paytan, A., Wortmann, U.G., 2018. Large-scale ocean deoxygenation during the Paleocene-Eocene Thermal Maximum. Science 361 (6404), 804–806.
Yi, Z., Huang, B., Chen, J., Chen, L., Wang, H., 2011. Paleomagnetism of early Paleogene marine sediments in southern Tibet, China: implications to onset of the India–Asia collision and size of Greater India. Earth Planet. Sci. Lett. 309 (1–2), 153–165.
Zachos, J., Pagani, M., Sloan, L., Thomas, E., Billups, K., 2001. Trends, rhythms, and aberrations in global climate 65 Ma to present. Science 292 (5517), 686–693.
Zachos, J.C., Röhl, U., Schellenberg, S.A., Sluijs, A., Hodell, D.A., Kelly, D.C., Thomas, E., Nicolo, M., Raffi, I., Lourens, L., McCarren, H., Kroon, D., 2005. Rapid acidification of the ocean during the Paleocene-Eocene thermal maximum. Science 308 (5728), 1611–1615.
Zerkle, A.L., Junium, C.K., Canfield, D.E., House, C.H., 2008. Production of ^{15}N-depleted biomass during cyanobacterial N_2-fixation at high Fe concentrations. J. Geophys. Res. Biogeosci. 113 (G3).
Zhai, R., Zeng, Z., Zhang, R., Yao, W., 2023. The response of nitrogen and sulfur cycles to ocean deoxygenation across the Cenomanian-Turonian boundary. Glob. Planet. Change 227, 104182.
Zhang, Q., Ding, L., Chen, X., Brennecka, G.A., Sun, Y., Ma, X., Gao, B., Zhang, Q., Willems, H., 2023. The large decline in carbonate $\delta^{238}U$ from a PETM section at Tingri, South Tibet, was driven by local sea-level changes, not global oceanic anoxia. Earth Planet. Sci. Lett. 612, 118164.
Zhang, X., Sigman, D.M., Morel, F.M., Kraepiel, A.M., 2014. Nitrogen isotope fractionation by alternative nitrogenases and past ocean anoxia. Proceedings of the National Academy of Sciences (USA) 111 (13), 4782–4787.